

51. PLOTS OF CROSS SECTIONS AND RELATED QUANTITIES

(For neutrino plots, see review article "Neutrino Cross Section Measurements" by G.P. Zeller in this edition of RPP)

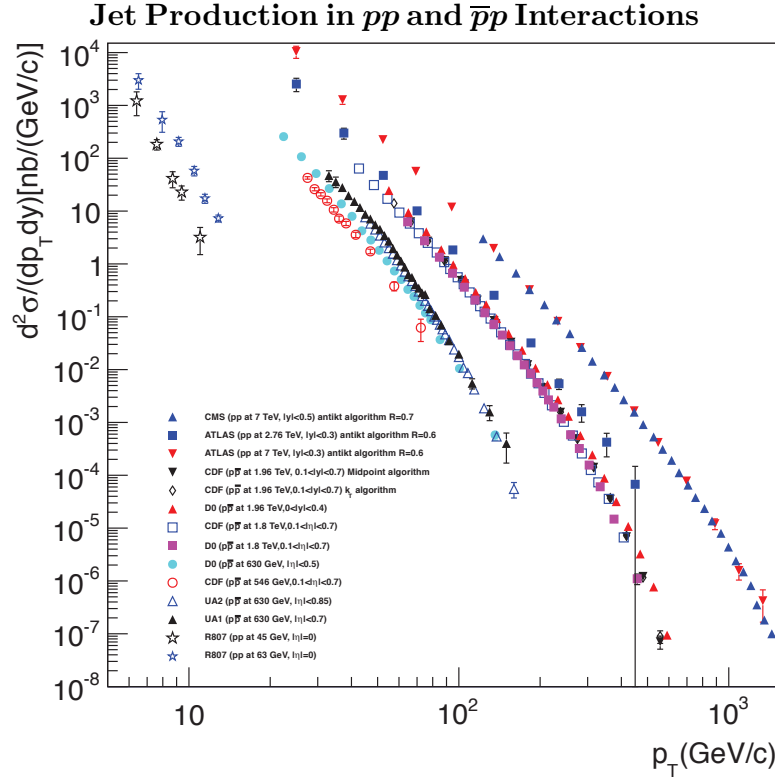


Figure 51.1: Inclusive differential jet cross sections, in the central rapidity region, plotted as a function of the jet transverse momentum. Results earlier than from the Tevatron Run 2 used transverse energy rather than transverse momentum and pseudo-rapidity η rather than rapidity y , but p_T and y are used for all results shown here for simplicity. The error bars plotted are in most cases the experimental stat. and syst. errors added in quadrature. The CDF and D0 measurements use jet sizes of 0.7 (JetClu for CDF Run 1, and Midpoint and k_T for CDF Run 2, a cone algorithm for D0 in Run 1 and the Midpoint algorithm in Run 2). The ATLAS results are plotted for the antikt algorithm for $R=0.4$, while the CMS results also use antikt, but with $R=0.5$. NLO QCD predictions in general provide a good description of the Tevatron and LHC data; the Tevatron jet data in fact are crucial components of global PDF fits, and the LHC data are starting to be used as well. Comparisons with the older cross sections are more difficult due to the nature of the jet algorithms used. **ATLAS:** Phys. Rev. **D86**, 014022 (2012), Eur. Phys. J **C73**, 2509 (2013); **CMS:** Phys. Rev. **D84**, 052011 (2011); **CDF:** Phys. Rev. **D75**, 092006 (2007), Phys. Rev. **D64**, 032001 (2001), Phys. Rev. Lett. **70**, 1376 (1993); **D0:** Phys. Rev. **D64**, 032003 (2001); **UA2:** Phys. Lett. **B257**, 232 (1991); **UA1:** Phys. Lett. **172**, 461 (1986); **R807:** Phys. Lett. **B123**, 133 (1983). (Courtesy of J. Huston, Michigan State University, 2013.)

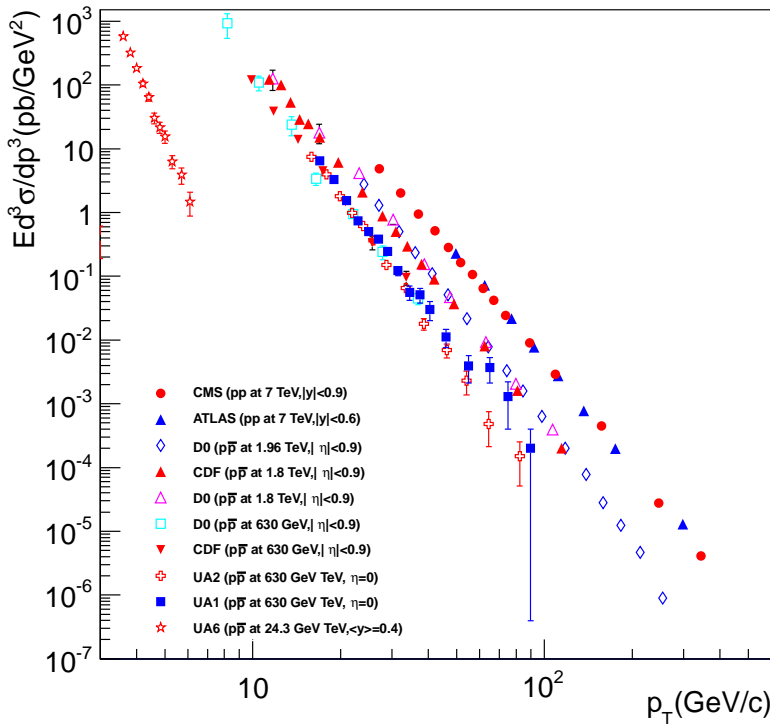
Direct γ Production in pp and $\bar{p}p$ Interactions

Figure 51.2: Isolated photon cross sections plotted as a function of the photon transverse momentum. The errors are either statistical only, or statistical and systematic added in quadrature. **ATLAS:** Phys. Lett. **B706**, 150 (2011); **CMS:** Phys. Rev. **D84**, 052011 (2011); **D0:** Phys. Lett. **B639**, 151 (2006), Phys. Rev. Lett. **87**, 251805 (2001); **CDF:** Phys. Rev. **D65**, 112003 (2002); **UA6:** Phys. Lett. **B206**, 163 (1988); **UA1:** Phys. Lett. **B209**, 385 (1988); **UA2:** Phys. Lett. **B288**, 386 (1992). (Courtesy of J. Huston, Michigan State University, 2013.)

Differential Cross Section for W and Z Boson Production

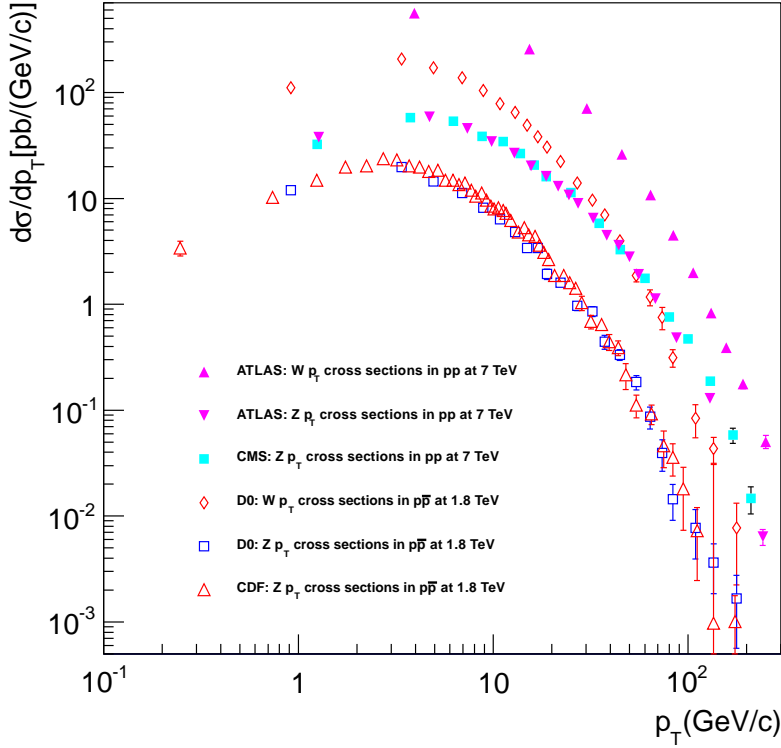


Figure 51.3: Differential cross sections for W and Z production shown as a function of the boson transverse momentum. The errors plotted are either statistical only or statistical and systematic added in quadrature. The results are in good agreement with theoretical predictions that include both the effects of NLO corrections and of q_T resummation. **ATLAS:** Phys. Rev. **D85**, 012005 (2012), Phys. Lett. **B705**, 415 (2011); **CMS:** Phys. Rev. **D85**, 032002 (2012); **D0:** Phys. Lett. **B513**, 292 (2001), Phys. Rev. Lett. **84**, 2792 (2000); **CDF:** Phys. Rev. Lett. **84**, 845 (2000). (Courtesy of J. Huston, Michigan State University, 2013.)

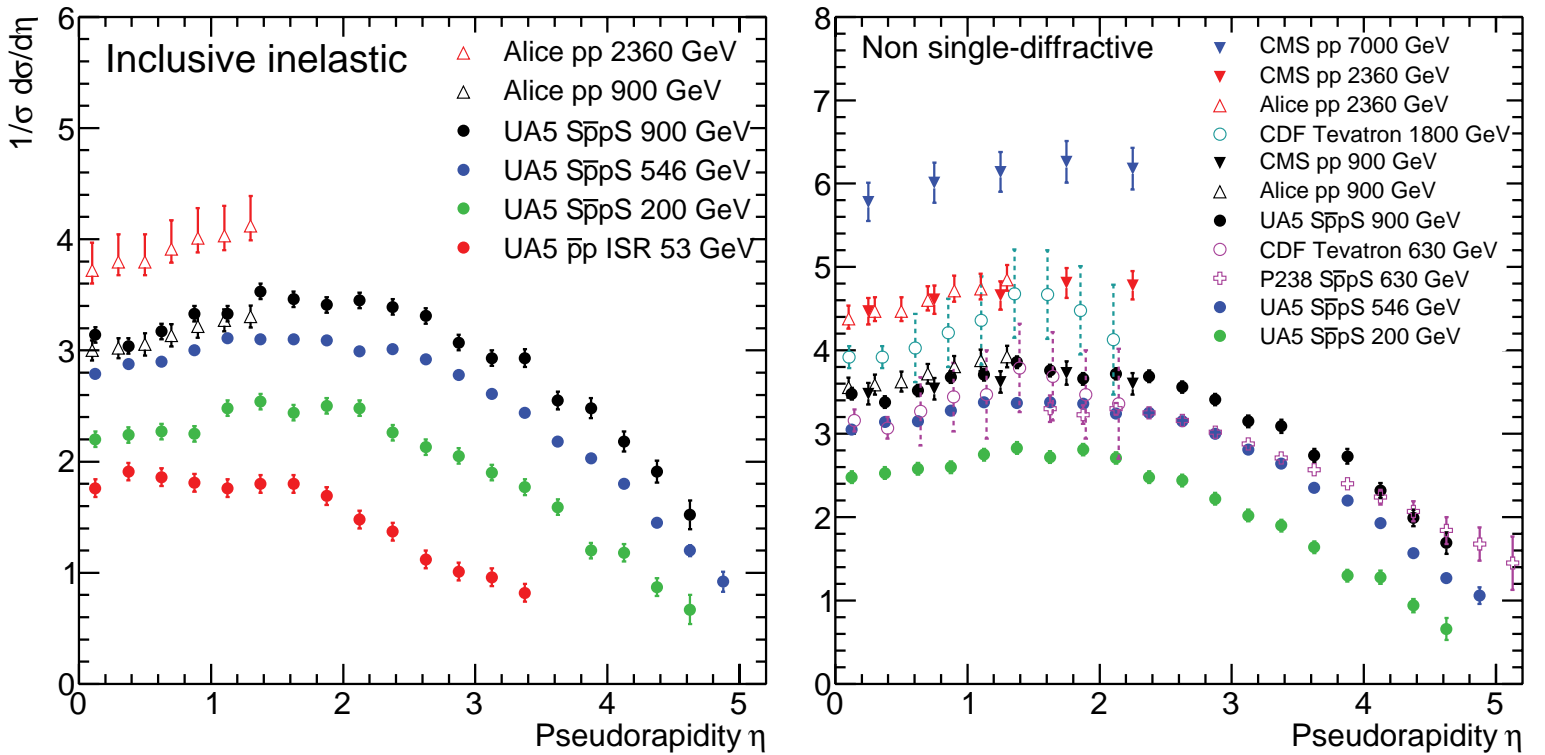
Pseudorapidity Distributions in pp and $p\bar{p}$ Interactions

Figure 51.4: Charged particle pseudorapidity distributions in pp collisions for $53 \text{ GeV} \leq \sqrt{s} \leq 1800 \text{ GeV}$. UA5 data from the $S\bar{p}pS$ are taken from G.J.Alner *et al.*, Z. Phys. **C33**, 1 (1986), and from the ISR from K.Alpgøard *et al.*, Phys.Lett. 112B 193 (1982). The UA5 data are shown for both the full inelastic cross-section and with singly diffractive events excluded. Additional non single-diffractive measurements are available from CDF at the Tevatron, F.Abe *et al.*, Phys. Rev. **D41**, 2330 (1990) and from P238 at the $S\bar{p}pS$, R.Harr *et al.*, Phys. Lett. **B401**, 176 (1997). These may be compared with both inclusive and non single-diffractive measurements in pp collisions at the LHC from ALICE, K.Aamodt *et al.*, Eur. Phys. J. **C68**, 89 (2010) and for non single-diffractive interactions from CMS, V.Khachatryan *et al.*, JHEP 1002:041 (2010), Phys. Rev. Lett. **105**, 022002 (2010). (Courtesy of D.R. Ward, Cambridge Univ., 2013)

Average Hadron Multiplicities in Hadronic e^+e^- Annihilation Events

Table 51.1: Average hadron multiplicities per hadronic e^+e^- annihilation event at $\sqrt{s} \approx 10, 29\text{--}35, 91,$ and $130\text{--}200$ GeV. The rates given include decay products from resonances with $c\tau < 10$ cm, and include the corresponding anti-particle state. Correlations of the systematic uncertainties were considered for the calculation of the averages. Quoted errors are not increased by scale factor S . (Updated August 2015 by O. Biebel, LMU, Munich)

| Particle | $\sqrt{s} \approx 10$ GeV | $\sqrt{s} = 29\text{--}35$ GeV | $\sqrt{s} = 91$ GeV | $\sqrt{s} = 130\text{--}200$ GeV |
|-----------------------------|-----------------------------|--------------------------------|------------------------------|----------------------------------|
| Pseudoscalar mesons: | | | | |
| π^+ | 6.52 ± 0.11 | 10.3 ± 0.4 | 17.02 ± 0.19 | 21.24 ± 0.39 |
| π^0 | 3.2 ± 0.3 | 5.83 ± 0.28 | 9.42 ± 0.32 | |
| K^+ | 0.953 ± 0.018 | 1.48 ± 0.09 | 2.228 ± 0.059 | 2.82 ± 0.19 |
| K^0 | 0.91 ± 0.05 | 1.48 ± 0.07 | 2.049 ± 0.026 | 2.10 ± 0.12 |
| η | 0.20 ± 0.04 | 0.61 ± 0.07 | 1.049 ± 0.080 | |
| $\eta'(958)$ | 0.03 ± 0.01 | 0.26 ± 0.10 | 0.152 ± 0.020 | |
| D^+ | $0.194 \pm 0.019^{(a)}$ | 0.17 ± 0.03 | 0.175 ± 0.016 | |
| D^0 | $0.446 \pm 0.032^{(a)}$ | 0.45 ± 0.07 | 0.454 ± 0.030 | |
| D_s^+ | $0.063 \pm 0.014^{(a)}$ | $0.45 \pm 0.20^{(b)}$ | 0.131 ± 0.021 | |
| $B^{(c)}$ | — | — | $0.134 \pm 0.016^{(d)}$ | |
| B^+ | — | — | $0.141 \pm 0.004^{(d)}$ | |
| B_s^0 | — | — | $0.054 \pm 0.011^{(d)}$ | |
| Scalar mesons: | | | | |
| $f_0(980)$ | 0.024 ± 0.006 | $0.05 \pm 0.02^{(e)}$ | 0.146 ± 0.012 | |
| $a_0(980)^\pm$ | — | — | $0.27 \pm 0.11^{(f)}$ | |
| Vector mesons: | | | | |
| $\rho(770)^0$ | 0.35 ± 0.04 | 0.81 ± 0.08 | 1.231 ± 0.098 | |
| $\rho(770)^\pm$ | — | — | $2.40 \pm 0.43^{(f)}$ | |
| $\omega(782)$ | 0.30 ± 0.08 | — | 1.016 ± 0.065 | |
| $K^*(892)^+$ | 0.27 ± 0.03 | 0.64 ± 0.05 | 0.714 ± 0.055 | |
| $K^*(892)^0$ | 0.29 ± 0.03 | 0.56 ± 0.06 | 0.738 ± 0.024 | |
| $\phi(1020)$ | 0.044 ± 0.003 | 0.085 ± 0.011 | 0.0963 ± 0.0032 | |
| $D^*(2010)^+$ | $0.177 \pm 0.022^{(a)}$ | 0.43 ± 0.07 | $0.1937 \pm 0.0057^{(g)}$ | |
| $D^*(2007)^0$ | $0.168 \pm 0.019^{(a)}$ | 0.27 ± 0.11 | — | |
| $D_s^*(2112)^+$ | $0.048 \pm 0.014^{(a)}$ | — | $0.101 \pm 0.048^{(h)}$ | |
| $B^* \text{ }^{(i)}$ | — | — | 0.288 ± 0.026 | |
| $J/\psi(1S)$ | $0.00050 \pm 0.00005^{(a)}$ | — | $0.0052 \pm 0.0004^{(j)}$ | |
| $\psi(2S)$ | — | — | $0.0023 \pm 0.0004^{(j)}$ | |
| $\Upsilon(1S)$ | — | — | $0.00014 \pm 0.00007^{(j)}$ | |
| Pseudovector mesons: | | | | |
| $f_1(1285)$ | — | — | 0.165 ± 0.051 | |
| $f_1(1420)$ | — | — | 0.056 ± 0.012 | |
| $\chi_{c1}(3510)$ | — | — | $0.0041 \pm 0.0011^{(j)}$ | |
| Tensor mesons: | | | | |
| $f_2(1270)$ | 0.09 ± 0.02 | 0.14 ± 0.04 | 0.166 ± 0.020 | |
| $f_2'(1525)$ | — | — | 0.012 ± 0.006 | |
| $K_2^*(1430)^+$ | — | 0.09 ± 0.03 | — | |
| $K_2^*(1430)^0$ | — | 0.12 ± 0.06 | 0.084 ± 0.022 | |
| $B^{** \text{ }^{(k)}}$ | — | — | 0.118 ± 0.024 | |
| D_{s1}^\pm | — | — | $0.0052 \pm 0.0011^{(\ell)}$ | |
| $D_{s2}^{*\pm}$ | — | — | $0.0083 \pm 0.0031^{(\ell)}$ | |
| Baryons: | | | | |
| p | 0.266 ± 0.008 | 0.640 ± 0.050 | 1.050 ± 0.032 | 1.41 ± 0.18 |
| Λ | 0.080 ± 0.007 | 0.205 ± 0.010 | 0.3915 ± 0.0065 | 0.39 ± 0.03 |
| Σ^0 | 0.023 ± 0.008 | — | 0.078 ± 0.010 | |
| Σ^- | — | — | 0.081 ± 0.010 | |
| Σ^+ | — | — | 0.107 ± 0.011 | |
| Σ^\pm | — | — | 0.174 ± 0.009 | |
| Ξ^- | 0.0059 ± 0.0007 | 0.0176 ± 0.0027 | 0.0262 ± 0.0009 | |
| $\Delta(1232)^{++}$ | 0.040 ± 0.010 | — | 0.085 ± 0.014 | |
| $\Sigma(1385)^-$ | 0.006 ± 0.002 | 0.017 ± 0.004 | 0.0240 ± 0.0017 | |
| $\Sigma(1385)^+$ | 0.005 ± 0.001 | 0.017 ± 0.004 | 0.0239 ± 0.0015 | |
| $\Sigma(1385)^\pm$ | 0.0106 ± 0.0020 | 0.033 ± 0.008 | 0.0472 ± 0.0027 | |
| $\Xi(1530)^0$ | 0.0015 ± 0.0006 | — | 0.00694 ± 0.00049 | |
| Ω^- | 0.0007 ± 0.0004 | 0.014 ± 0.007 | 0.00124 ± 0.00018 | |
| Λ_c^+ | $0.074 \pm 0.031^{(m)}$ | 0.110 ± 0.050 | 0.078 ± 0.017 | |
| Λ_b^0 | — | — | 0.031 ± 0.016 | |
| $\Sigma_c^{++}, \Sigma_c^0$ | 0.014 ± 0.007 | — | — | |
| $\Lambda(1520)$ | 0.008 ± 0.002 | — | 0.0222 ± 0.0027 | |

Notes for Table 51.1:

- (a) $\sigma_{\text{had}} = 3.33 \pm 0.05 \pm 0.21$ nb (CLEO: Phys. Rev. **D29**, 1254 (1984)) has been used in converting the measured cross sections to average hadron multiplicities.
- (b) $B(D_s \rightarrow \eta\pi, \eta'\pi)$ was used (RPP 1994).
- (c) Comprises both charged and neutral B meson states.
- (d) The Standard Model $B(Z \rightarrow b\bar{b}) = 0.217$ was used.
- (e) $x_p = p/p_{\text{beam}} > 0.1$ only.
- (f) Both charge states.
- (g) $B(D^*(2010)^+ \rightarrow D^0\pi^+) \times B(D^0 \rightarrow K^-\pi^+)$ has been used (RPP 2000).
- (h) $B(D_s^* \rightarrow D_s^+\gamma)$, $B(D_s^+ \rightarrow \phi\pi^+)$, $B(\phi \rightarrow K^+K^-)$ have been used (RPP 1998).
- (i) Any charge state (i.e., B_d^* , B_u^* , or B_s^*).
- (j) $B(Z \rightarrow \text{hadrons}) = 0.699$ was used (RPP 1994).
- (k) Any charge state (i.e., B_d^{**} , B_u^{**} , or B_s^{**}).
- (l) Assumes $B(D_{s1}^+ \rightarrow D^{*+}K^0 + D^{*0}K^+) = 100\%$ and $B(D_{s2}^+ \rightarrow D^0K^+) = 45\%$.
- (m) The value was derived from the cross section of $\Lambda_c^+ \rightarrow p\pi K$ using (a) and assuming the branching fraction to be $(5.0 \pm 1.3)\%$ (RPP 2004).

References for Table 51.1:

- RPP 1992:** Phys. Rev. **D45** (1992); **RPP 1994:** Phys. Rev. **D50**, 1173 (1994); **RPP 1996:** Phys. Rev. **D54**, 1 (1996); **RPP 1998:** Eur. Phys. J. **C3**, 1 (1998); **RPP 2000:** Eur. Phys. J. **C15**, 1 (2000); **RPP 2002:** Phys. Rev. **D66**, 010001 (2002); **RPP 2004:** Phys. Lett. **B592**, 1 (2004); **RPP 2006:** J. Phys. **G33**, 1 (2006); **RPP 2008:** Phys. Lett. **B667**, 1 (2008); **RPP 2010:** J. Phys. **G37**, 075021 (2010); **RPP 2012:** Phys. Rev. D 86,010001(2012) and references therein.
- R. Marshall, Rept. on Prog. in Phys. **52**, 1329 (1989). A. De Angelis, J. Phys. **G19**, 1233 (1993) and references therein.
- ALEPH:** D. Buskulic *et al.*: Phys. Lett. **B295**, 396 (1992); Z. Phys. **C64**, 361 (1994); **C69**, 15 (1996); **C69**, 379 (1996); **C73**, 409 (1997); and R. Barate *et al.*: Z. Phys. **C74**, 451 (1997); Phys. Reports **294**, 1 (1998); Eur. Phys. J. **C5**, 205 (1998); **C16**, 597 (2000); **C16**, 613 (2000); and A. Heister *et al.*: Phys. Lett. **B526**, 34 (2002); **B528**, 19 (2002).
- ARGUS:** H. Albrecht *et al.*: Phys. Lett. **230B**, 169 (1989); Z. Phys. **C44**, 547 (1989); **C46**, 15 (1990); **C54**, 1 (1992); **C58**, 199 (1993); **C61**, 1 (1994); Phys. Rep. **276**, 223 (1996).
- BaBar:** B. Aubert *et al.*: Phys. Rev. Lett. **87**, 162002 (2001); Phys. Rev. **D65**, 091104 (2002); J.P. Lees *et al.*: Phys. Rev. **D88**, 032011 (2013).
- Belle:** K. Abe *et al.*, Phys. Rev. Lett. **88**, 052001 (2002); and R. Seuster *et al.*, Phys. Rev. **D73**, 032002 (2006).
- CELLO:** H.J. Behrend *et al.*: Z. Phys. **C46**, 397 (1990); **C47**, 1 (1990).
- CLEO:** D. Bortoletto *et al.*, Phys. Rev. **D37**, 1719 (1988); erratum *ibid.* **D39**, 1471 (1989); and M. Artuso *et al.*, Phys. Rev. **D70**, 112001 (2004).
- Crystal Ball:** Ch. Bieler *et al.*, Z. Phys. **C49**, 225 (1991).
- DELPHI:** P. Abreu *et al.*: Z. Phys. **C57**, 181 (1993); **C59**, 533 (1993); **C61**, 407 (1994); **C65**, 587 (1995); **C67**, 543 (1995); **C68**, 353 (1995); **C73**, 61 (1996); Nucl. Phys. **B444**, 3 (1995); Phys. Lett. **B341**, 109 (1994); **B345**, 598 (1995); **B361**, 207 (1995); **B372**, 172 (1996); **B379**, 309 (1996); **B416**, 233 (1998); **B449**, 364 (1999); **B475**, 429 (2000); Eur. Phys. J. **C6**, 19 (1999); **C5**, 585 (1998); **C18**, 203 (2000); and J. Abdallah *et al.*, Phys. Lett. **B569**, 129 (2003); Phys. Lett. **B576**, 29 (2003); Eur. Phys. J. **C44**, 299 (2005); and W. Adam *et al.*: Z. Phys. **C69**, 561 (1996); **C70**, 371 (1996).
- HRS:** S. Abachi *et al.*, Phys. Rev. Lett. **57**, 1990 (1986); and M. Derrick *et al.*, Phys. Rev. **D35**, 2639 (1987).
- L3:** M. Acciarri *et al.*: Phys. Lett. **B328**, 223 (1994); **B345**, 589 (1995); **B371**, 126 (1996); **B371**, 137 (1996); **B393**, 465 (1997); **B404**, 390 (1997); **B407**, 351 (1997); **B407**, 389 (1997), erratum *ibid.* **B427**, 409 (1998); **B453**, 94 (1999); **B479**, 79 (2000).
- MARK II:** H. Schellman *et al.*, Phys. Rev. **D31**, 3013 (1985); and G. Wormser *et al.*, Phys. Rev. Lett. **61**, 1057 (1988).
- JADE:** W. Bartel *et al.*, Z. Phys. **C20**, 187 (1983); and D.D. Pietzl *et al.*, Z. Phys. **C46**, 1 (1990).
- OPAL:** R. Akers *et al.*: Z. Phys. **C63**, 181 (1994); **C66**, 555 (1995); **C67**, 389 (1995); **C68**, 1 (1995); and G. Alexander *et al.*: Phys. Lett. **B358**, 162 (1995); Z. Phys. **C70**, 197 (1996); **C72**, 1 (1996); **C72**, 191 (1996); **C73**, 569 (1997); **C73**, 587 (1997); Phys. Lett. **B370**, 185 (1996); and K. Ackerstaff *et al.*: Z. Phys. **C75**, 192 (1997); Phys. Lett. **B412**, 210 (1997); Eur. Phys. J. **C1**, 439 (1998); **C4**, 19 (1998); **C5**, 1 (1998); **C5**, 411 (1998); and G. Abbiendi *et al.*: Eur. Phys. J. **C16**, 185 (2000); **C17**, 373 (2000).
- PLUTO:** Ch. Berger *et al.*, Phys. Lett. **104B**, 79 (1981).
- SLD:** K. Abe, Phys. Rev. **D59**, 052001 (1999); Phys. Rev. **D69**, 072003 (2004).
- TASSO:** H. Aihara *et al.*, Z. Phys. **C27**, 27 (1985).
- TPC:** H. Aihara *et al.*, Phys. Rev. Lett. **53**, 2378 (1984).

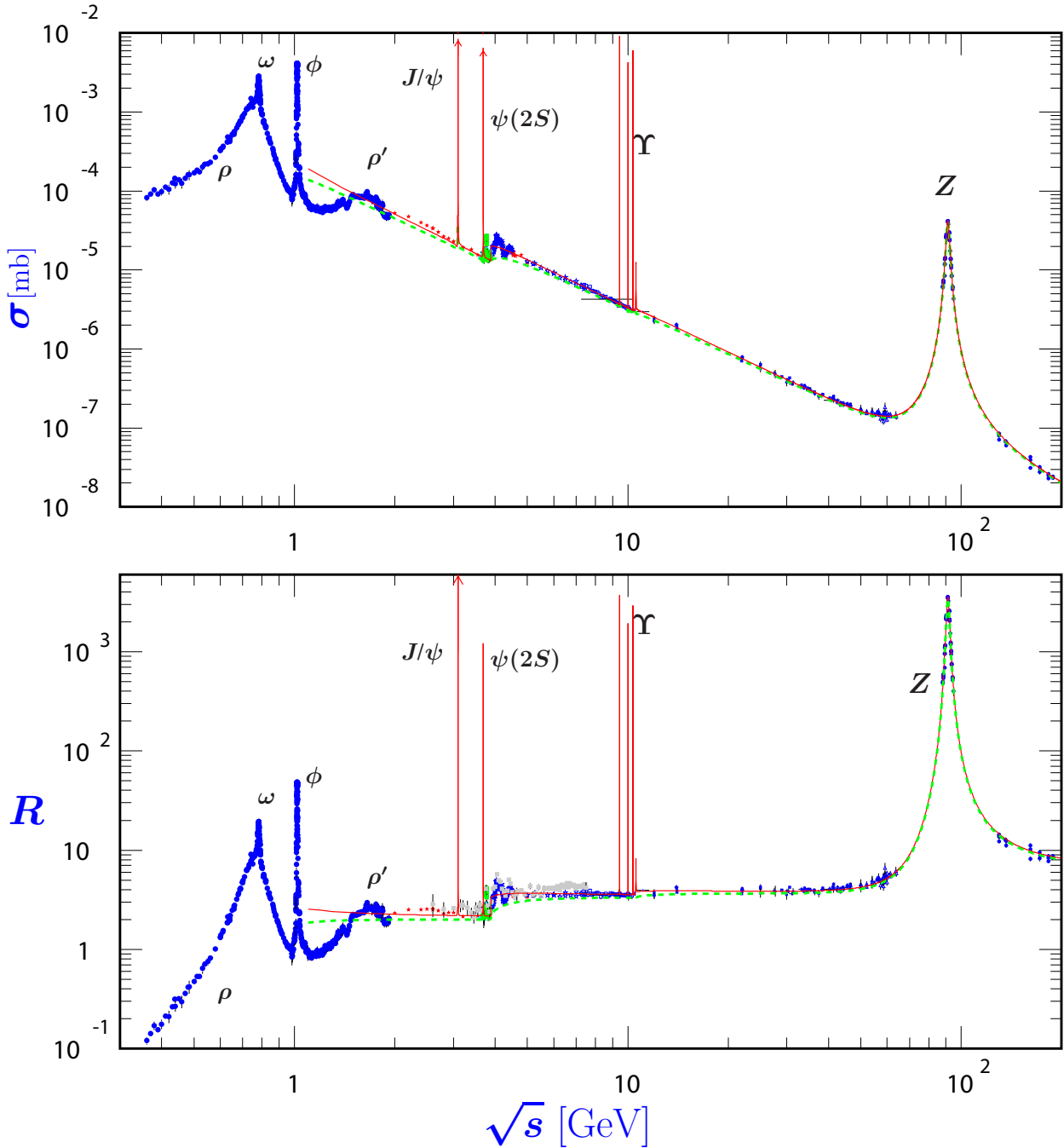
σ and R in e^+e^- Collisions

Figure 51.5: World data on the total cross section of $e^+e^- \rightarrow \text{hadrons}$ and the ratio $R(s) = \sigma(e^+e^- \rightarrow \text{hadrons}, s) / \sigma(e^+e^- \rightarrow \mu^+\mu^-, s)$. $\sigma(e^+e^- \rightarrow \text{hadrons}, s)$ is the experimental cross section corrected for initial state radiation and electron-positron vertex loops, $\sigma(e^+e^- \rightarrow \mu^+\mu^-, s) = 4\pi\alpha^2(s)/3s$. Data errors are total below 2 GeV and statistical above 2 GeV. The curves are an educative guide: the broken one (green) is a naive quark-parton model prediction, and the solid one (red) is 3-loop pQCD prediction (see “Quantum Chromodynamics” section of this Review, Eq. (9.7) or, for more details, K. G. Chetyrkin *et al.*, Nucl. Phys. **B586**, 56 (2000) (Erratum *ibid.* **B634**, 413 (2002))). Breit-Wigner parameterizations of J/ψ , $\psi(2S)$, and $\Upsilon(nS)$, $n = 1, 2, 3, 4$ are also shown. The full list of references to the original data and the details of the R ratio extraction from them can be found in [arXiv:hep-ph/0312114]. Corresponding computer-readable data files are available at <http://pdg.lbl.gov/current/xsect/>. (Courtesy of the COMPAS (Protvino) and HEPDATA (Durham) Groups, August 2015. Corrections by P. Janot (CERN) and M. Schmitt (Northwestern U.)

R in Light-Flavor, Charm, and Beauty Threshold Regions

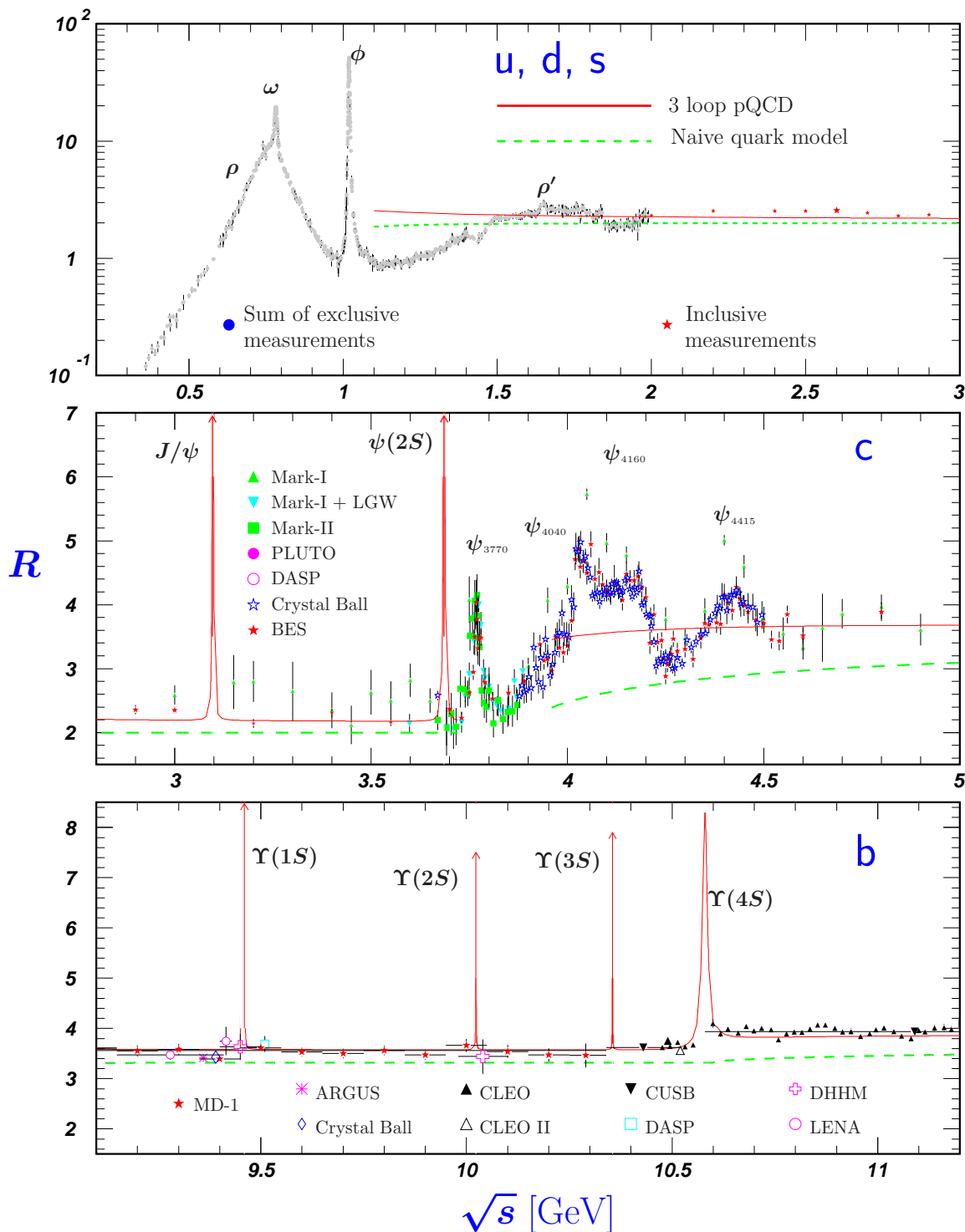


Figure 51.6: R in the light-flavor, charm, and beauty threshold regions. Data errors are total below 2 GeV and statistical above 2 GeV. The curves are the same as in Fig. 51.5. **Note:** CLEO data above $\Upsilon(4S)$ were not fully corrected for radiative effects, and we retain them on the plot only for illustrative purposes with a normalization factor of 0.8. The full list of references to the original data and the details of the R ratio extraction from them can be found in [arXiv:hep-ph/0312114]. The computer-readable data are available at <http://pdg.lbl.gov/current/xsect/>. (Courtesy of the COMPAS (Protvino) and HEPDATA (Durham) Groups, August 2015.)

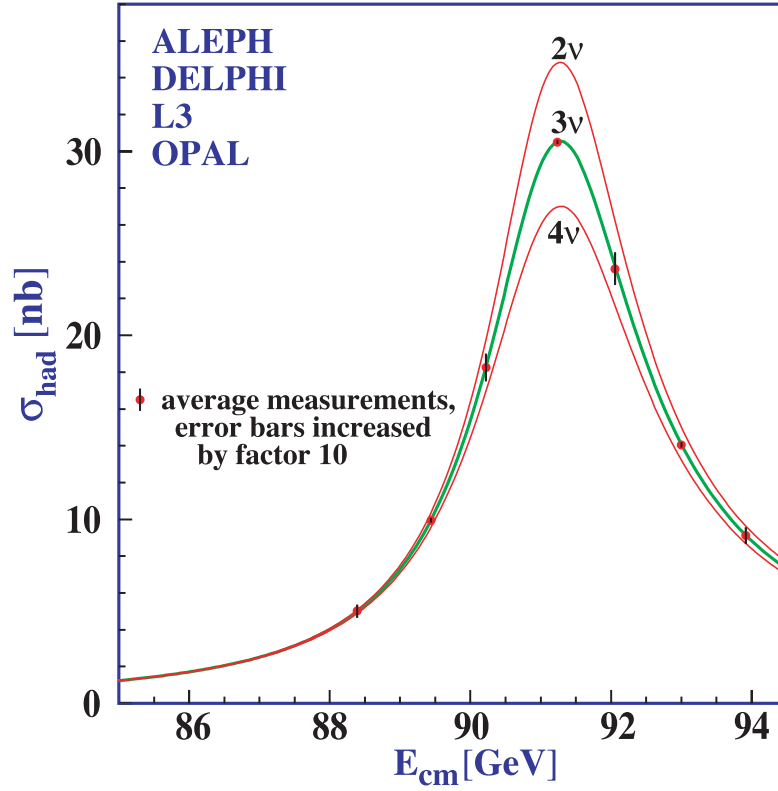
Annihilation Cross Section Near M_Z 

Figure 51.7: Combined data from the ALEPH, DELPHI, L3, and OPAL Collaborations for the cross section in e^+e^- annihilation into hadronic final states as a function of the center-of-mass energy near the Z pole. The curves show the predictions of the Standard Model with two, three, and four species of light neutrinos. The asymmetry of the curve is produced by initial-state radiation. Note that the error bars have been increased by a factor ten for display purposes. References:

ALEPH: R. Barate *et al.*, Eur. Phys. J. **C14**, 1 (2000).

DELPHI: P. Abreu *et al.*, Eur. Phys. J. **C16**, 371 (2000).

L3: M. Acciarri *et al.*, Eur. Phys. J. **C16**, 1 (2000).

OPAL: G. Abbiendi *et al.*, Eur. Phys. J. **C19**, 587 (2001).

Combination: The ALEPH, DELPHI, L3, OPAL, SLD Collaborations, the LEP Electroweak Working Group, and the SLD Electroweak and Heavy Flavor Groups, Phys. Rept. **427**, 257 (2006) [[arXiv:hep-ex/0509008](https://arxiv.org/abs/hep-ex/0509008)].

(Courtesy of M. Grünewald and the LEP Electroweak Working Group, 2007)

Total Hadronic Cross Sections

(Updated June 2016, COMPAS group, IHEP, Protvino)

This updated version of the total hadronic cross sections review is based on the first half of 2015 update of the database for total cross section and the ratio of the real-to-imaginary parts of the forward elastic scattering hadronic amplitudes. New data on total pp collisions cross sections from CERN-LHC-TOTEM [1–4] and CERN-LHC-ATLAS [5] were added.

We use a procedure for ranking models as described in [6] to identify the safest parameterizations for extrapolations. Incidentally, the models giving the best fit of accelerator data also reproduce the experimental cosmic ray nucleon–nucleon data extracted from nucleon–air data with no need of any extra phenomenological corrections to the data.

The statement in [6] that the models with universal (across of collision initial states) $B \log^2(s/s_0)$ asymptotic term work much better than the models with $B \log(s/s_0)$ or $B(s/s_0)^\Delta$ terms was confirmed in [7–11] based on matching traditional asymptotic parameterizations with low energy data in different ways. However in these references the scale parameter s_0 was still claimed to be dependent on the colliding particles as it should be for the asymptotic form of parameterizations constructed by the Regge-Gribov phenomenology prescriptions.

The possibility of the universal $\log^2(s/s_0)$ rise of the hadronic total cross sections for different colliding particles was first pointed out by W. Heisenberg [12–13] and discussed many times (see for example [14] and more recent [15–17], and references therein). In [16] the universality of the asymptotic total collision cross sections has been advocated for hadron-nucleus collisions. In [17] additional indications to the universal asymptotic high-energy behavior for hadronic total collision cross sections in form $B \log^2(s/s_0)$ were obtained from lattice QCD.

In this review we use HPR₁R₂ model of highest COMPETE-rank modified (as in 2012 version) to save the universality of the rising part in new form that explicitly includes dependence of the s_0 and B on the initial state mass parameters and the new scale parameter M .

$$\sigma^{a\bar{b}} = H \log^2 \left(\frac{s}{s_M} \right) + P^{ab} + R_1^{ab} \left(\frac{s}{s_M} \right)^{-\eta_1} \pm R_2^{ab} \left(\frac{s}{s_M} \right)^{-\eta_2};$$

$$\rho^{a\bar{b}} = \frac{1}{\sigma^{a\bar{b}}} \left[\pi H \log \left(\frac{s}{s_M} \right) - R_1^{ab} \left(\frac{s}{s_M} \right)^{-\eta_1} \tan \left(\frac{\eta_1 \pi}{2} \right) \pm R_2^{ab} \left(\frac{s}{s_M} \right)^{-\eta_2} \cot \left(\frac{\eta_2 \pi}{2} \right) \right],$$

where upper signs in formulas are for particles and lower signs for antiparticles. The adjustable parameters are as follows:

$H = \pi \frac{(\hbar c)^2}{M^2}$ in mb, where notation H^\S is after Heisenberg(1952,1975);

P^{ab} in mb, are Pomeranchuk's(1958) constant terms;

R_i^{ab} in mb are the intensities of the effective secondary Regge pole contributions named after Regge-Gribov(1961);

$s, s_M^{ab} = (m_a + m_b + M)^2$ are in GeV^2 ;

$m_a, m_b, (m_{\gamma^*} = m_{\rho(770)})$ are the masses of initial state particles, and M – the mass parameter defining the rate of universal rise of the cross sections are all in GeV . Parameters M, η_1 and η_2 are universal for all collisions considered.

Exact factorization hypothesis was used for both $H \log^2(\frac{s}{s_M})$ and P^{ab} to extend the universal rise of the total hadronic cross sections to the $\gamma(p, d) \rightarrow \text{hadrons}$ and $\gamma\gamma \rightarrow \text{hadrons}$ collisions. This results in one additional adjustable parameter δ with substitutions:

$$\pi H \log^2 \left(\frac{s}{s_M^{\gamma(p,d)}} \right) + P^{\gamma(p,d)} \Rightarrow \delta \left[\pi(1, \lambda) H \log^2 \left(\frac{s}{s_M^{\gamma(p,d)}} \right) + P^{\gamma(p,d)} \right];$$

$$\pi H \log^2 \left(\frac{s}{s_M^{\gamma\gamma}} \right) + P^{\gamma\gamma} \Rightarrow \delta^2 \left[\pi H \log^2 \left(\frac{s}{s_M^{\gamma\gamma}} \right) + P^{\gamma\gamma} \right].$$

These parameterizations were used for simultaneous fit with **35** adjustable parameters to the data on collisions:

$$(\bar{p}, p) (p, n, d); \quad \Sigma^- p; \quad \pi^\mp (p, n, d); \quad K^\mp (p, n, d); \quad \gamma p; \quad \gamma \gamma; \quad \gamma d.$$

The results of the fits are presented in the following table and figures. In the table, two values of the fit quality indicator $\text{FQ} = \chi^2/(\text{Npt} - 35)$ are reported in the last element of the first row, where **Npt** is the number of data points in corresponding sample. FQ_{INT} calculated with “internal” parameter values of machine precision (16 digits) and FQ_{EXT} calculated with rounded parameter values as displayed in the table in accordance with PDG rules (Section 5.3 of J. Beringer *et al.*, (Particle Data Group), Phys. Rev. **D86**, 010001 (2012)), recent metrology recommendations [18] and rules for safe uniform rounding of correlated data [19]. The uniformity of the quality of data description across different collisions is shown in the last two columns of the table; **npt** is the number of data points in a subsample and χ^2/npt is the contribution of the subsample to the global χ^2 reduced to **npt**.

^{\S}For collisions with deuteron target $H_d = \lambda H$ where dimensionless parameter λ is introduced to test the universality of the Heisenberg rise for particle–nuclear and nuclear–nuclear collisions.

| HPR₁R₂ at $\sqrt{s} \geq 5\text{GeV}$ | M=2.1206 ± 0.0094 [GeV] H=0.2720 ± 0.0024 [mb] | | FQ _{INT} = 0.96 FQ _{EXT} = 0.96 | | |
|-----------------------------------------------------------------------|-------------------------------------------------------------------------|--------------------------|------------------------------------------------------|-----------------|------------------------------------------|
| | $\eta_1 = 0.4473 \pm 0.0077$ $\eta_2 = 0.5486 \pm 0.0049$ | | | | |
| | $\delta = (3.063 \pm 0.014) \times 10^{-3}$ $\lambda = 1.624 \pm 0.033$ | | | | |
| P[mb] | R₁[mb] | R₂[mb] | Beam/Target | Npt=1048 | χ^2/npt by Groups |
| 34.41 ± 0.13 | 13.07 ± 0.17 | 7.394 ± 0.081 | $\bar{p}(p)/p$ | 258 | 1.14 |
| 34.71 ± 0.17 | 12.52 ± 0.34 | 6.66 ± 0.15 | $\bar{p}(p)/n$ | 67 | 0.48 |
| 34.7 ± 1.3 | -46. ± 18. | -48. ± 18. | Σ^-/p | 9 | 0.37 |
| 18.75 ± 0.11 | 9.56 ± 0.15 | 1.767 ± 0.030 | π^\mp/p | 183 | 1.02 |
| 16.36 ± 0.09 | 4.29 ± 0.13 | 3.408 ± 0.044 | K^\mp/p | 121 | 0.82 |
| 16.31 ± 0.10 | 3.70 ± 0.19 | 1.826 ± 0.068 | K^\mp/n | 64 | 0.58 |
| | 0.0139 ± 0.0011 | | γ/p | 41 | 0.62 |
| | $(-4. \pm 17.) \times 10^{-6}$ | | γ/γ | 37 | 0.75 |
| | 0.0370 ± 0.0019 | | γ/d | 13 | 0.9 |
| 64.45 ± 0.32 | 29.66 ± 0.39 | 14.94 ± 0.18 | $\bar{p}(p)/d$ | 85 | 1.52 |
| 36.65 ± 0.26 | 18.75 ± 0.36 | 0.341 ± 0.091 | π^\mp/d | 92 | 0.72 |
| 32.06 ± 0.19 | 7.70 ± 0.31 | 5.616 ± 0.082 | K^\mp/d | 78 | 0.79 |

To construct the parameter scatter region we follow Section 39.4.2.2 of J. Beringer *et al.* (Particle Data Group), Phys. Rev. **D86**, 010001 (2012) and recent metrology JCGM 101:2008 recommendations and produce the direct Monte Carlo propagation of uncertainties from experimental data to the uncertainties of the best fit parameters. To do this we interpret the whole input data sample as statistically independent sample with total experimental uncertainty at each experimental data point being a Gaussian standard deviation. This technical assumption allows us to generate MC sampling of experimental data and to obtain at each MC trial new “biased” best fit parameters belonging to scatter region of the initial best fit parameters values. These biased best fit parameters constitute the MC-samples of cardinalities $|MC_{cut}|$ at each \sqrt{s} cutoff and are the basis for construction of three 35-dimensional empirical parameter distributions.

In paper [19] the asymptotic bounds (Froissart, Martin) on the possible rise of the total collision cross sections in the form $\log^2(s/s_0)$ was questioned in favour of possible faster rising forms. It was supported by the fits presented in [18] where the form $\log^c(s/s_0)$ with adjustable c was tested on $(\bar{p})pp$ data only and it was claimed that values of c obtained in number of different fits are statistically compatible with $c \in [2.2, 2.4]$.

We have performed our global fit with adjustable c to the total cross sections and available ρ -parameters (as of August 2015) including TOTEM data point at 8 TeV [20]. For this fit we have 36 adjustable parameters. Fit was done with all data at $\sqrt{s} \geq 5$ GeV with $FQ = 0.87$. We have obtained value $c = 1.98 \pm 0.01$ (Hessian error) which is in two standard deviation lower than $c = 2$ (exact) and possibly could be tentatively interpreted as an indication to the slower universal rising total cross sections as it was proposed 45 years ago by Cheng and Wu in the form $\log^2\left(\frac{(s/s_0)^a}{\log^2(s/s_0)}\right)$ in their seminal paper [21]. However, to notice this difference much experimental, theoretical, and modelling work has to be done.

In conclusion, the Heisenberg prediction of the universal $\log^2(s/s_M)$ form of asymptotic rise of the hadronic collision total cross sections is still actual and should be tested in all aspects at available colliders operating with $(\bar{p}, p, \text{nucl}ei)$ beams and in experiments with cosmic rays.

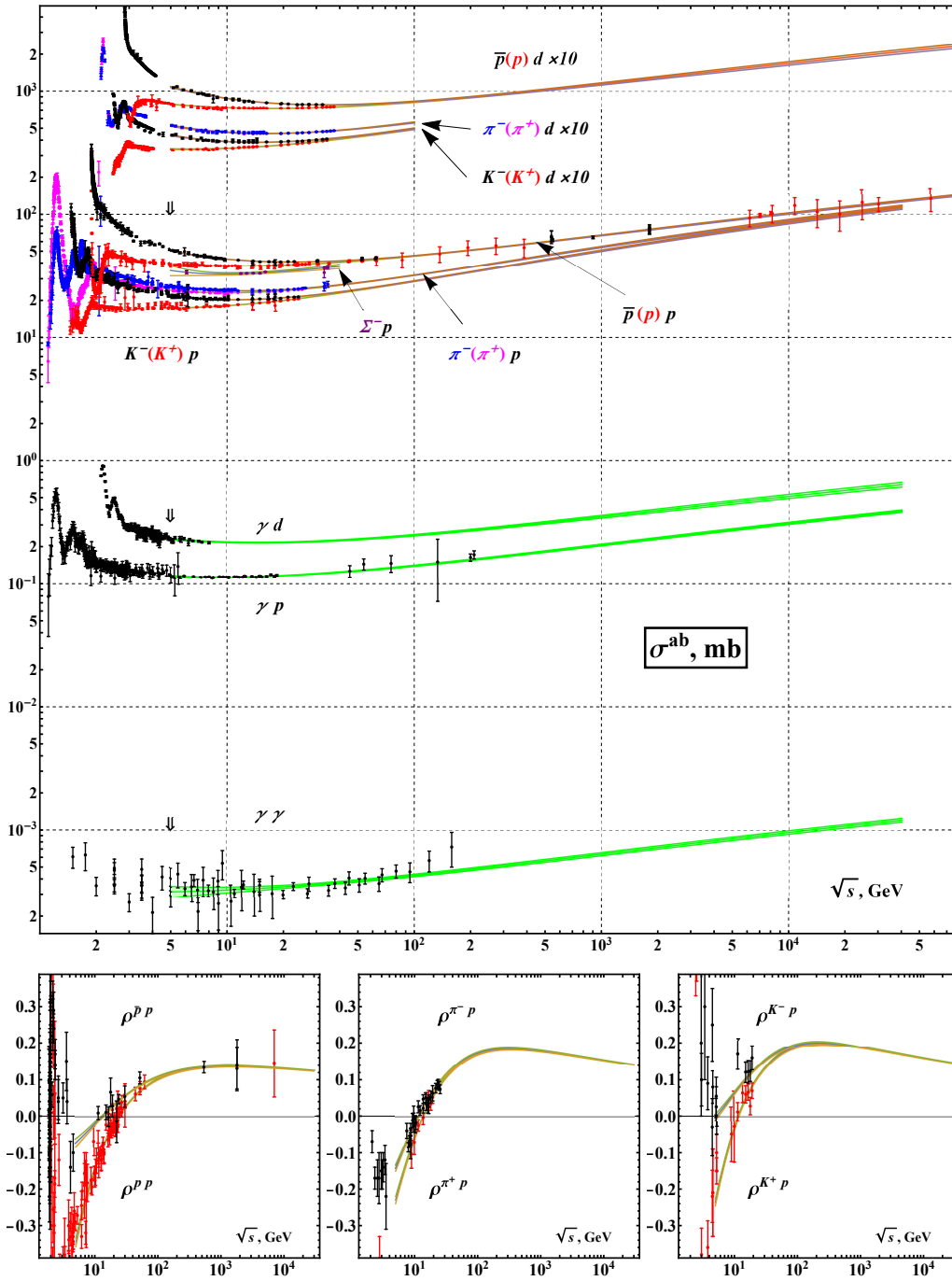


Figure 51.8: Summary of $h^\mp p \rightarrow \text{anything}$, $\gamma p \rightarrow \text{hadrons}$, $\gamma\gamma \rightarrow \text{hadrons}$ total cross sections σ^{ab} in mb and $\rho^{h^\mp p}$ the ratio of real to imaginary parts of the forward hadronic amplitudes. Also for qualitative comparison of the uniformity of data description by HPR₁R₂-model across the different collisions and observables. The uncertainties for the experimental data points include both the statistical and systematic errors. Curves, corresponding to fit above 5 GeV cut, are plotted with error bands calculated with parameter covariance matrix constructed on MC-propagated vectors from 95% quantile of the empirical distribution.

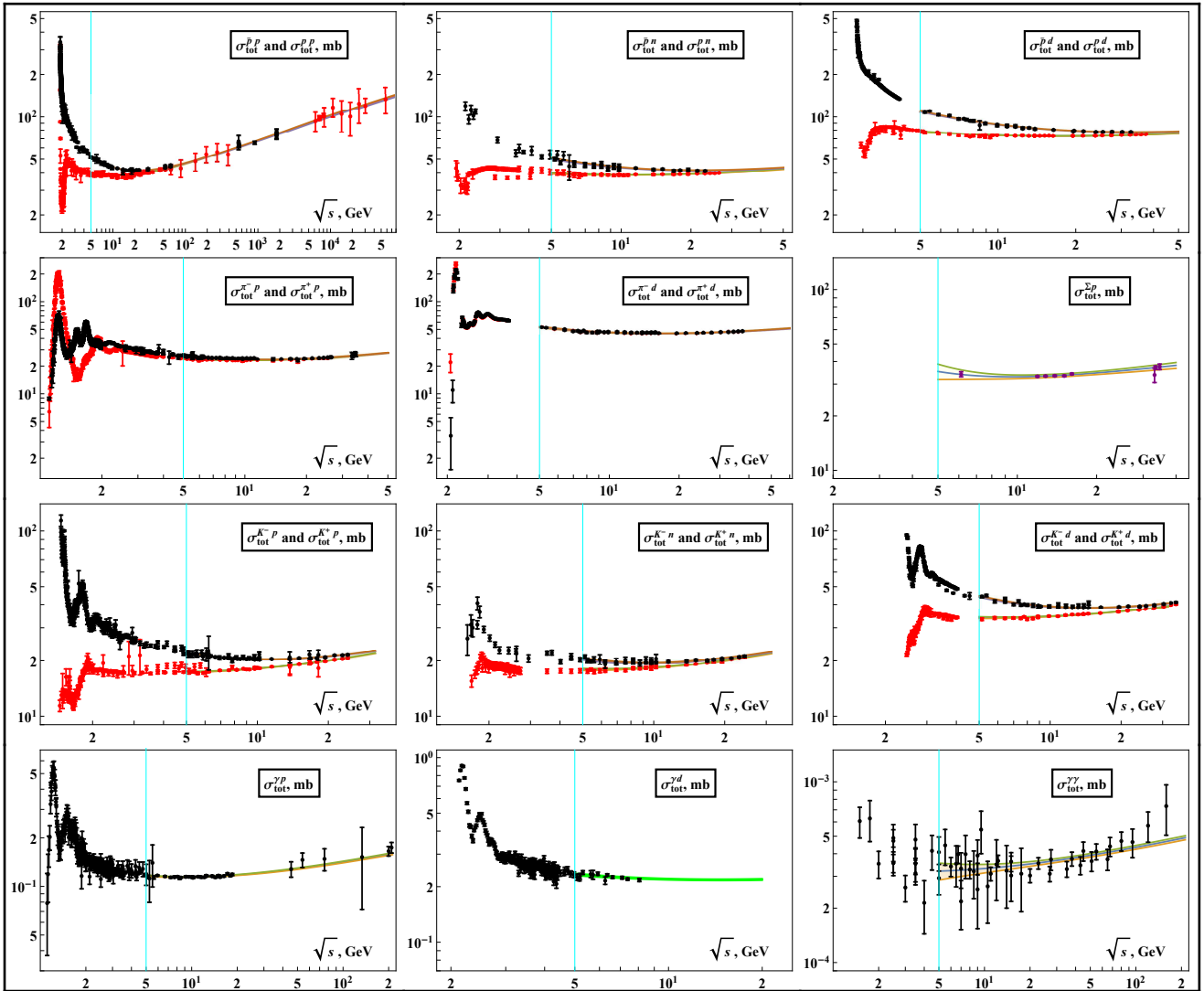


Figure 51.9: Summary of all total collision cross sections jointly fitted with available hadronic ρ parameter data. Corresponding computer-readable data files may be found at <http://pdg.lbl.gov/xsect/contents.html>

References

- [1] G. Antchev *et al.*, Nucl. Phys. **B899**, 527 (2013).
- [2] G. Antchev *et al.*, Phys. Rev. Lett. **111**, 012001 (2013).
- [3] G. Antchev *et al.*, Europhys. Lett. **101**, 21004 (2013).
- [4] G. Antchev *et al.*, Europhys. Lett. **101**, 21002 (2013).
- [5] G. Aad *et al.*, Nucl. Phys. **B889**, 486 (2014).
- [6] J.R. Cudell *et al.*: Phys. Rev. **D65**, 074024 (2002); Phys. Rev. Lett. **89**, 201801 (2002).
- [7] K. Igi and M. Ishida: Phys. Rev. **D66**, 034023 (2002); Phys. Lett. **B622**, 286 (2005).
- [8] M.M. Block and F. Halzen: Phys. Rev. **D72**, 036006 (2005); Phys. Rev. **D72**, 039902 (2005).
- [9] M. Ishida and K. Igi, Prog. Theor. Phys. Suppl. **187**, 297 (2011).
- [10] M. Ishida and V. Barger, Phys. Rev. **D84**, 014027 (2011).
- [11] F. Halzen *et al.*, Phys. Rev. **D85**, 074020 (2012).
- [12] W. Heisenberg, Z. Phys. **133**, 65 (1952).
- [13] W. Heisenberg, *Fourteenth Int. Cosm. Ray Conference*, Vol.11, München 1975, 3461-3474;
- [14] S.S. Gershtein and A.A. Logunov, Sov. J. Nucl. Phys. **39**, 960 (1984).
- [15] E. Iancu and R. Venugopalan, R.C. Hwa (ed.) *et al.*, [hep-ph/0303204].
- [16] L. Frankfurt, M. Strikman, and M. Zhalov, Phys. Lett. **B616**, 59 (2005).
- [17] M. Giordano, E. Meggiolaro, and N. Moretti, JHEP **1209**, 031 (2012).
- [18] JCGM 100:2008, JCGM 101:2008, JCGM 104:2009, JCGM 102:2011 via www.bipm.org/en/publications/guides/gum.html
- [19] V.V. Ezhela, Data Science Journal **6**, PS676 (2007).
- [20] Y.I. Azimov, Phys. Rev. **D84**, 056012 (2011).
- [21] D.A. Fagundes, M.J. Menon, and P.V.R.G. Silva, J. Phys. **G40**, 065005 (2013).
- [22] H. Cheng and T.T. Wu, Phys. Rev. Lett. **24**, 1456 (1970).

High Energy Elastic $\bar{p}p$ and pp Differential Cross Sections

(Updated June 2016, COMPAS group, IHEP, Protvino)

Using new results from FNAL-COLLIDER-D0 experiment in $\bar{p}p$ elastic collisions at $\sqrt{s} = 1.96$ TeV [1], CERN-LHC-TOTEM, CERN-LHC-ATLAS experiments in pp elastic collisions at $\sqrt{s} = 7, 8$ TeV [2-3] and PAO experiment in proton-air collisions at 57 TeV [4] the amplitudes of the elastic $\bar{p}p$ and pp collisions are investigated in a most broad region in \sqrt{s} and t via three observables $d\sigma/dt(s, t)$, $\sigma^{tot}(s)$, and $\rho(s)$. The summary of the database for $d\sigma/dt(s, t)$ is presented in Figure 51.10, where projection of the $d\sigma/dt(\sqrt{s}, t)$ to the $(d\sigma/dt, -t)$ plane orthogonal to the \sqrt{s} axis is displayed.

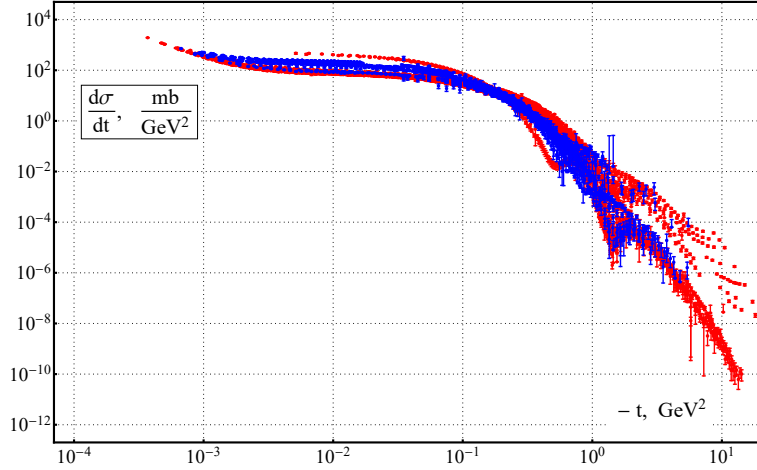


Figure 51.10: Cumulative plots of data on $d\sigma/dt$ for $\bar{p}p$ (blue) and pp (red) elastic collisions at $\sqrt{s} \geq 2.99$ GeV. Number of data points $N_{pt} = 6629$

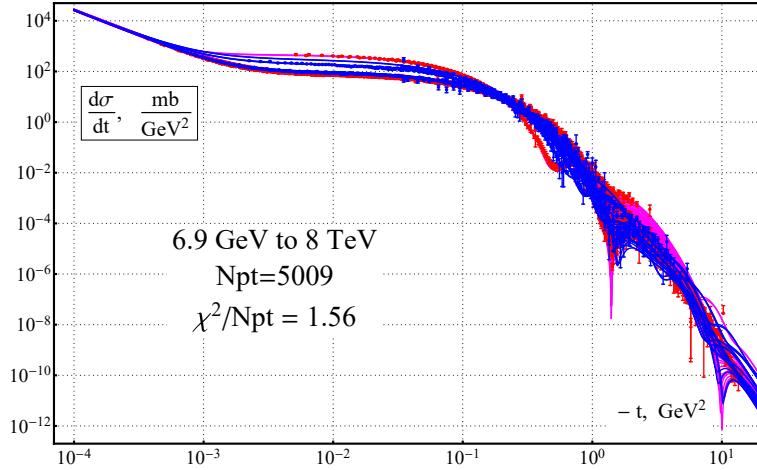


Figure 51.11: Cumulative plots of data on $d\sigma/dt$ and model description for $\bar{p}p$ (blue,blue) and pp (red,magenta) elastic collisions at $\sqrt{s} \geq 6.9$ GeV.

All characteristic features of the $d\sigma/dt(\sqrt{s}, t)$ behavior in $-t$ and \sqrt{s} are clearly seen:

- The energy-dependent Coulomb-Nuclear Interference (CNI) effects at small $-t$;
- Diffractive peaks with crossover effect at $-t \approx 0.16$ GeV² for particle-antiparticle data at same energies;
- The first dip/shoulder moving to the left with growing \sqrt{s} . New data on $d\sigma/dt$ in $\bar{p}p$ and pp elastic collisions at highest accelerator energies have challenged all previous model predictions that gave “not so bad qualitative agreement” with previously available data on $d\sigma/dt$. There is a need to reveal a quantitative and statistically complete picture of the data description by at least one model with most ambitious claim on the “best known description”. There are several conceptually related papers with such a claims [5–7] but with different areas of applicability and without treatment of the CNI region. Description of $d\sigma/dt$ by our model (a variation of AGNM [7] parameterization) at $\sqrt{s} \geq 6.9$ GeV is displayed on Figure 51.11.

Historically the most complete compilations on $d\sigma/dt$ data expressed in Mandelstam variables \sqrt{s} and t were published in Landolt-Börnstein volumes (now available in digital form) up to 1981 [8]. Updated (in high energy part) analogous CLM-compilation [9] (available in computer readable form) was compiled with help of HEPDATA and COMPAS databases and released in 2006. In our fits we use the CLM-compilation with minor corrections, filled detected gaps, and updated with new data published up to August 2015. We performed simultaneous fits to the sample of data on $d\sigma/dt(s, t)$, $\sigma^{tot}(s)$, and $\rho(s)$ in $\bar{p}p$ and pp collisions at $6.9 \text{ GeV} \leq \sqrt{s} \leq 8 \text{ TeV}$ and all available t . Overall fit quality $FQ = \chi^2(N_{pt})/(5266 - 37) = 1.60$, which is unreliable for our number of degrees of freedom. Removing contributions to $\chi^2(d\sigma/dt)$ from $N_{out} = 277$ points with $\chi^2(\text{point}) > (2.4)^2$ (of $2.4 \times \text{standard deviation (std)}$ – randomly scattered outliers) we have $\chi^2(N_{rest})/(N_{rest}) = 1.02$, where $N_{rest} = N_{pt}(d\sigma/dt) - N_{out}$. The uniformity level of the fit quality in different intervals of \sqrt{s} is shown on Figure 51.12.

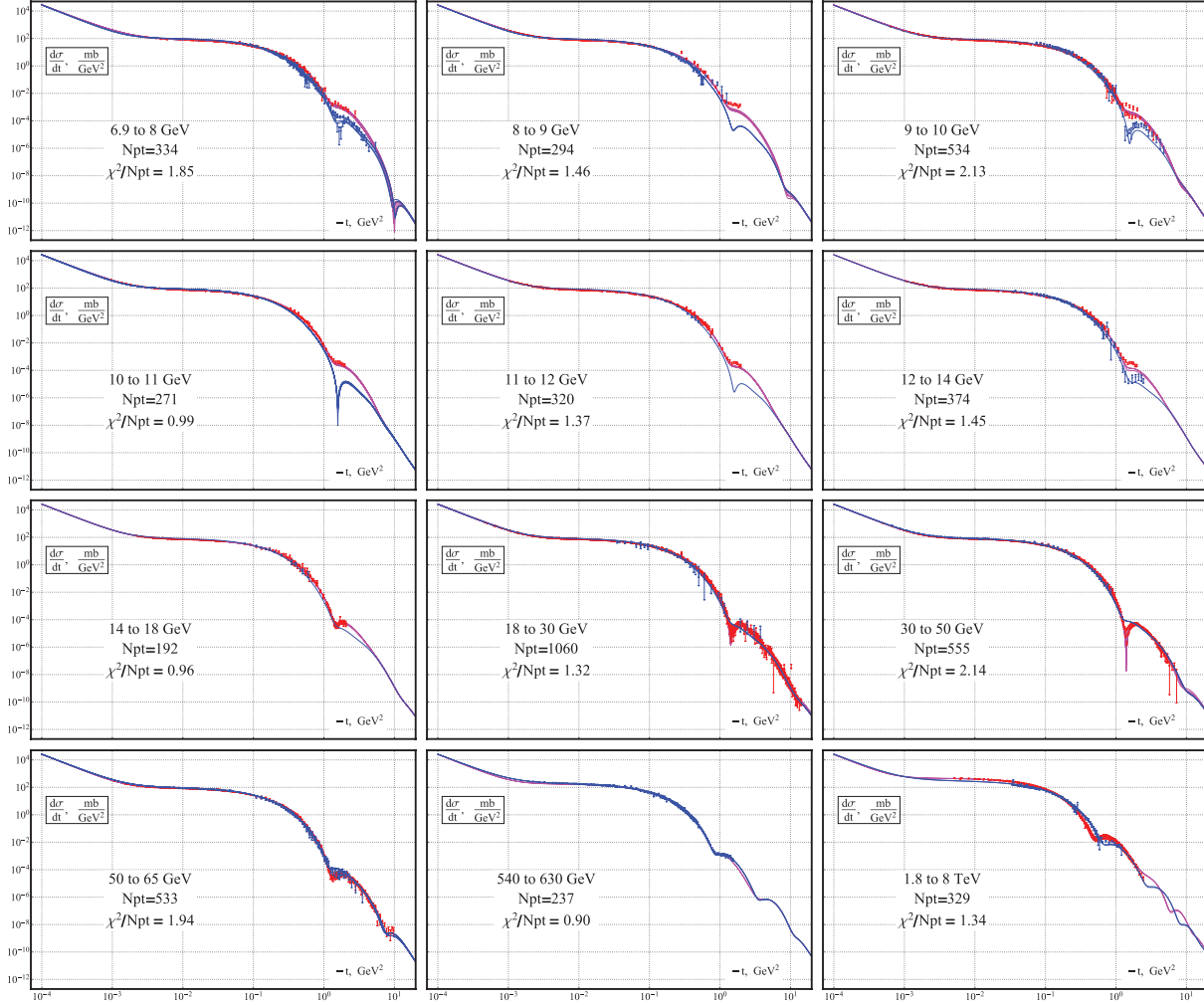


Figure 51.12: All 12 energy intervals are non-overlapping and cover all data points. All panels have axis labelled as in Figure 51.11. All data sets corresponding to the same energy have model curve drawn. Some panels have no red or blue data points. In such a cases we add the curve as prediction of the model.

To reveal a more complete picture of phenomenological description of the elastic scattering data we originally selected the most flexible model (43 parameters) from [7] with most broad claimed area of applicability. It turns out that without partial removal of some data (made in [7]) the claimed solution cannot be used even as starting point for adjustments, most probably, because of over-rounded published parameter values, or misprints in parameter tables, or strong parameter correlations. Moreover, numerous fits with different starting points failed to find any locally stable solution with physically reasonable adjustable parameter values. We obtain a stable solution only with addition of data in CNI region and with slightly modified parameterization to reduce the number of adjustable parameters from 43 to 37. Our expressions for observables $\sigma_{\pm}^{tot}(s)$, $\rho_{\pm}(s)$, and $d\sigma_{\pm}/dt(s, t)$ with sign “+” for pp and sign “-” for $\bar{p}p$ collisions are constructed (in notations of [7]) using corresponding scattering amplitudes: nuclear $T_{\pm}(s, t)$ and Coulomb $T_{\pm}^c(s, t)$ both in $\text{mb} \cdot \text{GeV}^2$ as follows:

$$\sigma_{\pm}^{tot}(s) = \frac{\text{Im } T_{\pm}(s, 0)}{\sqrt{s(s - 4m_p^2)}}, \quad \rho_{\pm}(s) = \frac{\text{Re } T_{\pm}(s, 0)}{\text{Im } T_{\pm}(s, 0)}, \quad \frac{d\sigma_{\pm}}{dt}(s, t) = \frac{|T_{\pm}(s, t) + T_{\pm}^c(s, t)|^2}{16\pi(\hbar c)^2 s(s - 4m_p^2)},$$

where constants: m_p stands for proton mass, and $(\hbar c)^2$ for mb-to-GeV² conversion factor. Nuclear amplitudes $T_{\pm}(s, t)$ are linearly combined crossing even $F_+(\hat{s}, t)$ and crossing odd $F_-(\hat{s}, t)$ functions.

$$T_{\pm}(s, t) = [F_+(\hat{s}, t) \pm F_-(\hat{s}, t)],$$

$$F_+(\hat{s}, t) = F_+^H(\hat{s}, t) + F_+^P(\hat{s}, t) + F_+^{PP}(\hat{s}, t) + F_+^R(\hat{s}, t) + F_+^{RP}(\hat{s}, t) + N_+(s, t),$$

$$F_-(\hat{s}, t) = F_-^{MO}(\hat{s}, t) + F_-^O(\hat{s}, t) + F_-^{OP}(\hat{s}, t) + F_-^R(\hat{s}, t) + F_-^{RP}(\hat{s}, t) + N_-(s, t),$$

$$F_+^H(\hat{s}, t) = i\hat{s} \left\{ \begin{array}{l} H_1 \frac{2J_1(K_+\tilde{\tau})}{K_+\tilde{\tau}} \cdot e^{b_+1t} \ln^2 \tilde{s} + \\ H_2 J_0(K_+\tilde{\tau}) \cdot e^{b_+2t} \ln \tilde{s} + \\ H_3 [J_0(K_+\tilde{\tau}) - K_+\tilde{\tau} J_1(K_+\tilde{\tau})] \cdot e^{b_+3t} \end{array} \right\}, \quad F_-^{MO}(\hat{s}, t) = \hat{s} \left\{ \begin{array}{l} O_1 \frac{\sin(K_-\tilde{\tau})}{K_-\tilde{\tau}} e^{b_-1t} \cdot \ln^2 \tilde{s} + \\ O_2 \cos(K_-\tilde{\tau}) e^{b_-2t} \cdot \ln \tilde{s} + \\ O_3 e^{b_-3t} \end{array} \right\},$$

$$\begin{aligned}
 F_+^P(\hat{s}, t) &= -C_P e^{b_P t} e^{-i\frac{\pi}{2}\alpha_P(t)} (\hat{s})^{\alpha_P(t)}, & F_-^O(\hat{s}, t) &= iC_O e^{b_O t} e^{-i\frac{\pi}{2}\alpha_O(t)} (\hat{s})^{\alpha_O(t)} (1 + A_O t), \\
 F_+^{PP}(\hat{s}, t) &= -\frac{C_{PP}}{\ln \hat{s}} e^{b_{PP} t} e^{-i\frac{\pi}{2}\alpha_{PP}(t)} (\hat{s})^{\alpha_{PP}(t)}, & F_-^{OP}(\hat{s}, t) &= i\frac{C_{OP}}{\ln \hat{s}} e^{b_{OP} t} e^{-i\frac{\pi}{2}\alpha_{OP}(t)} (\hat{s})^{\alpha_{OP}(t)}, \\
 F_{\pm}^{RP}(\hat{s}, t) &= \frac{iC_{RP}^{\pm}}{\ln \hat{s}} e^{b_{RP}^{\pm} t} e^{-i\frac{\pi}{2}\alpha_{RP}^{\pm}(t)} (\hat{s})^{\alpha_{RP}^{\pm}(t)}, & F_{\pm}^R(\hat{s}, t) &= \mp C_R^{\pm} e^{b_R^{\pm} t} e^{-i\frac{\pi}{2}\alpha_R^{\pm}(t)} (\hat{s})^{\alpha_R^{\pm}(t)}, \\
 N_{\pm}(s, t) &= -i^{\frac{1\pm 1}{2}} \cdot \hat{s} \cdot N_{\pm} \cdot (\ln \hat{s}) \frac{t}{t_0} \cdot (1 - t/t_{\pm})^{-5}, \\
 \alpha_P(t) &= 1 + \alpha'_P \cdot t; & \alpha_R^{\pm}(t) &= \alpha_R^{\pm}(0) + \alpha_R^{\pm\prime} \cdot t; & \alpha_O(t) &= 1 + \alpha'_O \cdot t, \\
 \alpha_{OP}(t) &= 1 + \frac{\alpha'_P \alpha'_O}{\alpha'_P + \alpha'_O} \cdot t; & \alpha_{PP}(t) &= 1 + \frac{\alpha'_P}{2} \cdot t; & \alpha_{RP}^{\pm}(t) &= \alpha_R^{\pm}(0) + \frac{\alpha_P' \alpha_R^{\pm\prime}}{\alpha_P' + \alpha_R^{\pm\prime}} \cdot t,
 \end{aligned}$$

$$\hat{s}(s, t) \equiv \hat{s} = (-t + 2s - 4m_p^2)/(2s_0), \quad s_0 = 1 \text{ GeV}^2; \quad \ln(\hat{s}) = \ln(s) - i\frac{\pi}{2}; \quad \tilde{\tau} = \sqrt{-t/t_0} \ln \hat{s}, \quad t_0 = 1 \text{ GeV}^2.$$

Coulomb amplitudes are taken with dipole electric nucleon form factor

$$T_{\pm}^c(s, t) = \mp e^{[\pm i\alpha\Phi_{\pm}^{NC}(s, t)]} \cdot 8\pi(\hbar c)^2 \alpha \cdot \frac{s}{t} \cdot \left(1 - \frac{t}{\Lambda^2}\right)^{-4},$$

where: $\Phi_{\pm}^{CN}(s, t) = \ln \left[-\frac{t}{2} \left(B_{\pm}(s) + \frac{8}{\Lambda^2} \right) \right] + \gamma - \frac{4t}{\Lambda^2} \ln \left(-\frac{4t}{\Lambda^2} \right) - \frac{2t}{\Lambda^2}$ is the CNI phase in the R. Cahn form [10]; $\Lambda = \sqrt{0.71} \text{ GeV}$; α – fine structure constant; γ – Euler constant. Instead of the traditional definition of the $d\sigma_{\pm}/dt(s, t)$ slope function $B_{\pm}(s) = \left[\frac{d}{dt} \ln \left(\frac{d\sigma_{\pm}}{dt}(s, t) \right) \right]_{t=0}$, we set $B_{\pm}(s) = \frac{\sigma_{\pm}(s)}{4\pi(\hbar c)^2}$ to simplify calculations and to get faster minimization procedures. The odderon contribution at $t = 0$ can be switched off by replacing all exponents $e^{b_i t}$ by $e^{b_i t}(1 - e^{-t/t_{min}})$ in the above expressions for all odderon related terms, where t_{min} is the minimal $|t|$ -value for which the data exist in the $d\sigma/dt$ database. The resulting non-intersecting $\sigma_{\mp}(\sqrt{s})$ and $\rho_{mp}(\sqrt{s})$ curves can be obtained without significant degradation to the fit quality [11]. The effect of switching odderon contribution on and off at $t = 0$ is shown in Figure 51.13.

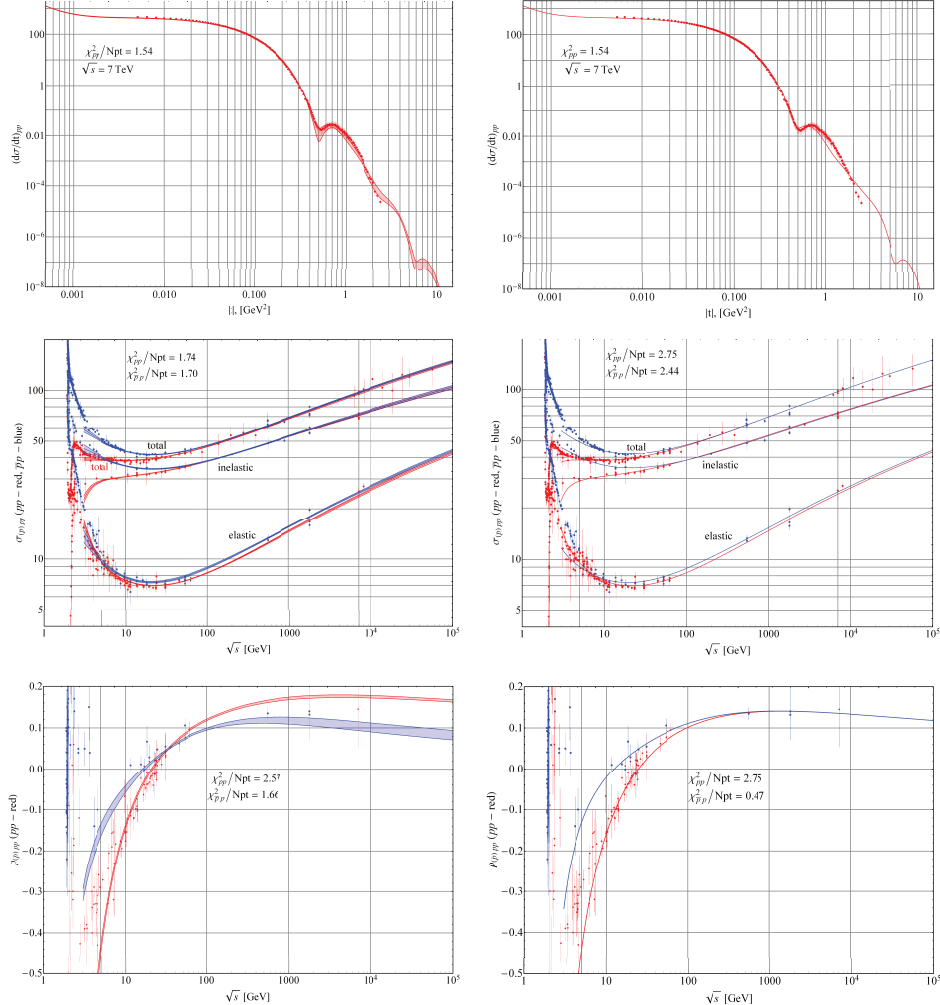


Figure 51.13: Comparisons of $d\sigma/dt$ at $\sqrt{s} = 7\text{TeV}$, $d\sigma^{tot}$, and $\rho(\sqrt{s})$ data with our two variants of AGNM [7] models. Right-hand panels have odderons switched off at $t = 0$. Curves for integrated elastic cross sections and inelastic cross sections were obtained from integration of the elastic differential cross sections. Data from experiments are not used in the fits.

The best fit parameter values and their standard deviations for both models are listed in the tables below. The table on the left (right) is with (without) oderon contribution. Estimates of the std were obtained by the MC-propagation of the assumed Gaussian distribution for each individual data point. Despite of poor MC statistics, the obtained “propagated” covariance matrix is in good conditions and gives reasonable std estimates. The quality of the fit to the $\sigma_{\mp}^{tot}(s)$ and $\rho_{\mp}(s)$ data is presented in Figure 51.13. Error bands were calculated by propagation of the parameter scatter region to the scatter region of these observables.

| Name | Unit | Value | \pm Vstd | Name | Unit | Value | \pm Vstd | Name | Unit | Value | \pm Vstd | Name | Unit | Value | \pm Vstd | | | | | | |
|----------------------------------------------------------------------------------|---------------------|------------|--------------|-----------------|---------------------|------------|--------------|-------------------|---------------------|---------------------|-----------------------------------------------------------------------------------------------------------|-----------------|---------------------|------------|--------------|--|--|--|-------------------|------------|--------------|
| H_1 | mb GeV ² | 0.2488 | 0.0008 | O_1 | mb GeV ² | 0. | (fix) | H_1 | mb GeV ² | 0.2525 | 0.0005 | O_1 | mb GeV ² | 0. | (fix) | | | | | | |
| H_2 | mb GeV ² | 0.00691 | 0.00041 | O_2 | mb GeV ² | 0.576 | 0.026 | H_2 | mb GeV ² | 0.002545 | 0.000095 | O_2 | mb GeV ² | 0.576 | 0.004 | | | | | | |
| H_3 | mb GeV ² | 10.42 | 0.17 | O_3 | mb GeV ² | -3.256 | 0.160 | H_3 | mb GeV ² | 9.51 | 0.05 | O_3 | mb GeV ² | -3.256 | 0.003 | | | | | | |
| K_+ | | 0.3092 | 0.0010 | K_- | | 0.1000 | 0.0012 | K_+ | | 0.3164 | 0.0035 | K_- | | 0.1000 | 0.0008 | | | | | | |
| C_P | mb GeV ² | -0.0946 | 0.0058 | C_O | mb GeV ² | -6.91 | 0.27 | C_P | mb GeV ² | -0.2661 | 0.0040 | C_O | mb GeV ² | -6.910 | 0.032 | | | | | | |
| C_{PP} | mb GeV ² | 159.80 | 1.44 | C_{OP} | mb GeV ² | 53.83 | 1.12 | C_{PP} | mb GeV ² | 171.80 | 0.75 | C_{OP} | mb GeV ² | 53.83 | 0.06 | | | | | | |
| C_{R}^+ | mb GeV ² | -30.20 | 1.04 | C_{R}^- | mb GeV ² | 85.10 | 1.79 | C_{R}^+ | mb GeV ² | -41.84 | 0.62 | C_{R}^- | mb GeV ² | 85.10 | 0.06 | | | | | | |
| C_{RP}^+ | mb GeV ² | -1.897 | 0.124 | C_{RP}^- | mb GeV ² | -48.77 | 2.77 | C_{RP}^+ | mb GeV ² | -0.511 | 0.087 | C_{RP}^- | mb GeV ² | -48.7700 | 0.0021 | | | | | | |
| $\alpha_R^+(0)$ | | 0.651 | 0.009 | $\alpha_R^-(0)$ | | 0.4558 | 0.0060 | $\alpha_R^+(0)$ | | 0.628 | 0.006 | $\alpha_R^-(0)$ | | 0.4558 | 0.0060 | | | | | | |
| $\alpha_R'^+$ | GeV ⁻² | 0.8 | (fix) | $\alpha_R'^-$ | GeV ⁻² | 0.8 | (fix) | $\alpha_R'^+$ | GeV ⁻² | 0.8 | (fix) | $\alpha_R'^-$ | GeV ⁻² | 0.8 | (fix) | | | | | | |
| α'_P | GeV ⁻² | 0.1603 | 0.0052 | α'_O | GeV ⁻² | 0.680 | 0.033 | α'_P | GeV ⁻² | 0.2461 | 0.0013 | α'_O | GeV ⁻² | 0.680 | 0.026 | | | | | | |
| b_{+1} | GeV ⁻² | 3.895 | 0.029 | b_{-1} | GeV ⁻² | 0. | (fix) | b_{+1} | GeV ⁻² | 4.017 | 0.008 | b_{-1} | GeV ⁻² | 0. | (fix) | | | | | | |
| b_{+2} | GeV ⁻² | 0.608 | 0.011 | b_{-2} | GeV ⁻² | 2.935 | 0.037 | b_{+2} | GeV ⁻² | 0.457 | 0.005 | b_{-2} | GeV ⁻² | 2.935 | 0.014 | | | | | | |
| b_{+3} | GeV ⁻² | 6.45 | 0.10 | b_{-3} | GeV ⁻² | 2.502 | 0.028 | b_{+3} | GeV ⁻² | 7.63 | 0.02 | b_{-3} | GeV ⁻² | 2.502 | 0.004 | | | | | | |
| b_P | GeV ⁻² | 0.0801 | 0.0291 | b_O | GeV ⁻² | 14.75 | 0.31 | b_P | GeV ⁻² | $b_P \rightarrow 0$ | 0 | b_O | GeV ⁻² | 14.75 | 0.05 | | | | | | |
| b_{PP} | GeV ⁻² | 5.287 | 0.034 | b_{OP} | GeV ⁻² | 2.480 | 0.030 | b_{PP} | GeV ⁻² | 4.808 | 0.007 | b_{OP} | GeV ⁻² | 2.480 | 0.007 | | | | | | |
| b_R^+ | GeV ⁻² | 1.928 | 0.062 | b_R^- | GeV ⁻² | 9.25 | 0.22 | b_R^+ | GeV ⁻² | 1.596 | 0.012 | b_R^- | GeV ⁻² | 9.25 | 0.07 | | | | | | |
| b_{RP}^+ | GeV ⁻² | 0.4525 | 0.0215 | b_{RP}^- | GeV ⁻² | 1.154 | 0.039 | b_{RP}^+ | GeV ⁻² | 0.3862 | 0.0050 | b_{RP}^- | GeV ⁻² | 1.154 | 0.005 | | | | | | |
| N_+ | mb GeV ² | -0.0773 | 0.0043 | N_- | mb GeV ² | 15.93 | 1.54 | N_+ | mb GeV ² | -0.0508 | 0.0014 | N_- | mb GeV ² | 15.93 | 0.84 | | | | | | |
| t_+ | GeV ² | 1.475 | 0.021 | t_- | GeV ² | 0.1221 | 0.0088 | t_+ | GeV ² | 1.700 | 0.013 | t_- | GeV ² | 0.1221 | 0.0011 | | | | | | |
| FQ_{INT} = 1.598; FQ_{EXT} = 1.604; with oderon | | | | A_{OP} | | | | GeV ⁻² | 0.0 | (fix) | FQ_{INT} = 1.648; FQ_{EXT} = 1.694; without oderon (at $t=0$) | | | | A_{OP} | | | | GeV ⁻² | 0.0 | (fix) |
| | | | | A_O | | | | GeV ⁻² | -34.72 | 2.01 | | | | | A_O | | | | GeV ⁻² | -34.72 | 0.52 |

FQ_{INT} calculated with “internal” parameter values of machine precision (16 digits) and FQ_{EXT} calculated with rounded parameter values as displayed in the table in accordance with PDG rules.

In summary, the solution obtained gives satisfactory picture of the used parametric description of the current database on observables related to elastic (anti)proton–proton scattering amplitudes, and reveals problems with lack of good data at the pre-asymptotic energies. Indeed:

- Noisy data in dip/shoulder regions does not allow to tune parameters to give credible description of the depth of dips;
- All frames in Figure 51.12 with $\sqrt{s} \leq 12$ GeV apparently show that there is an urgent need in $\bar{p}p$ data at CNI as well as at the first dip/shoulder “ $-t$ ” intervals;
- Frame marked as “9 to 10 GeV” shows some contradictory data samples in pp collisions (48 “2.4–std outliers” out of 565 data points). There are no model independent resolution of these contradictions other than remeasurements with much higher statistics and more precise measuring systems. New accurate experimental data are highly desirable;
- There is a sharp difference in descriptions of ρ parameter data from our global fits with HPR₁R₂ model without oderon contribution (non-intersecting ρ_{\mp} curves) and our variant of AGNM model [7] with oderons (intersecting ρ_{\mp} curves). Further modelling is needed to remove this difference. Another issue to note is that the $\rho_-(\sqrt{s})$ curve is consistently above the $\rho_+(\sqrt{s})$ curve with a constant offset (see Figure 19 in [12]);
- The 277 ($> 2.4\sigma$) outliers contribute to about one third of the total χ^2 for the 5009 experimental data points. This issue is not fully understood but may indicate that the procedure of removing some “uncomfortable data” [11,13-15] should be examined more carefully.

References

- [1] V.M. Abazov *et al.*, Phys. Rev. **D86**, 012009 (2012);
- [2] G. Antchev *et al.*, Nucl. Phys. B **899**, 527 (2015); Phys. Rev. Lett. **111**, 012001 (2013); Europhys. Lett.: **101**, 21004 (2013); **101**, 21002 (2013); **96**, 21002 (2011); **95**, 41001 (2011).
- [3] G. Aad *et al.*, Nucl. Phys. B **889**, 486 (2014).
- [4] P. Abreu *et al.*, Phys. Rev. Lett. **109**, 062002 (2012).
- [5] R. Avila, P. Gauron, and B. Nicolescu, Eur. Phys. J. **C49**, 581 (2007).
- [6] E. Martynov, Phys. Rev. **D76**, 074030 (2007).
- [7] E. Martynov and B. Nicolescu, Eur. Phys. J. **C56**, 57 (2008).
- [8] In Landolt-Börnstein, Group I: P.J. Carson, v.9, 675 (1980); R.R. Shubert, v.9, 216 (1980); P.J. Carlson, v.7, 109 (1973); A.N. Diddens, v.7, 27 (1973).
- [9] J. R. Cudell, A. Lengyel, and E. Martynov, Phys. Rev. **D73**, 034008 (2006).
- [10] R. Cahn, Z. Phys. **C15**, 253 (1982).
- [11] E. Martynov, Phys. Rev. **D87**, 114018 (2013).
- [12] O.V. Selyugin, Phys. Rev. **D91**, 113003 (2015).
- [13] A. Donnachie and P.V. Landshoff, Phys. Lett. **B727**, 500 (2013).
- [14] A.A. Godizov, Phys. Lett. **B735**, 57 (2014).
- [15] A. Donnachie and P.V. Landshoff, Int. J. Mod. Phys. **A29**, 1446007 (2014).